An All-Digital Low-Power Structural Health Monitoring System

Jina Kim[1], Benjamin L. Grisso[2], Dong S. Ha[1], and Daniel J. Inman[2]

VTVT (Virginia Tech VLSI for Telecommunications) Lab[1]
Department of Electrical and Computer Engineering
Virginia Tech, Blacksburg, VA 24061-0111
{jikim4, ha}@vt.edu

Center for Intelligent Material Systems and Structures[2]
Department of Mechanical Engineering
Virginia Tech, Blacksburg, VA 24061-0261
{begrisso, dinman}@vt.edu

***Abstract*—Structural health monitoring is desirable in many fields to provide a means of damage detection on a variety of structures. Unfortunately, the ability to equip structures with health monitoring systems is limited by the development of adequate hardware. Previously, prototypes using the impedance-based health monitoring method have been developed to lay a foundation for permanent structural damage detection. These prototypes served their purposes, but has shortcomings such that large size and high power consumption. In this paper, all-digital excitation and sensing techniques are developed to reduce both the size and power dissipation. The digital techniques are implemented onto a new prototype, which achieves substantial reduction in size and power consumption. Validation of the new hardware on a representative structure is presented and compared with traditional techniques for structural health monitoring.**

I. Introduction

Permanent deployment of the structural health monitoring (SHM) systems onto real world structures is gaining increased attention, and consequently autonomous sensor technology becomes critical. The two most essential aspects to developing autonomous SHM systems are self-contained hardware implementation and low power dissipation.

Traditionally, a sinusoidal single tone has been used to excite the structure of interest, and the response is measured in terms of voltage. The sinusoidal signal frequency gradually increases until the entire frequency range is excited. After measuring the structural response, the measured voltage undergoes a fast Fourier transform (FFT) to provide impedance values at each frequency component. This frequency sweeping excitation method is highly time and power consuming, as each frequency component in the target frequency range must be individually excited.

Thus, we proposed our first approach to shorten the excitation time, and resultantly reduce the power dissipation, using an impulse-like sinc excitation signal [1][2]. Frequency components from DC to half the digital-to-analog converter (DAC) sampling frequency are overlaid in time domain to generate a sinc waveform that requires only $1/N_{freq}$ excitation time while covering the entire target frequency range, where N_{freq} is the number of frequency components in the target frequency range. Though we have reduced the excitation time and lowered the power dissipation accordingly, the power hungry hardware elements required for structural excitation remain.

Therefore, we have suggested another approach to eliminate one of the power hungry hardware elements [3]. To eliminate the DAC, an excitation method employing a noise-like digital wideband (DW) signal, which is generated from a pseudo noise (PN) sequence covering the bandwidth of the target frequency range and up-converted to the center of the target frequency range, was proposed. Besides the reduced power dissipation compared to the sinc excitation signal, the DW excitation signal also reduced the memory requirements. Since the DW excitation signal is a random digital sequence, the excitation signal does not have to be stored for repetitive excitation, while the sinc excitation signal had to be stored in memory.

In this paper, we present our latest approach involving digital rectangular pulse train (DRPT) excitation signals and sample-based detection to eliminate a power hungry analog-to-digital converter (ADC) as well as a DAC. Though both the DW and DRPT excitation signals are digital sequences, the DRPT excitation signal has an advantage over the DW excitation signal because generating DRPT signals with known frequencies requires less clock cycles and no complicated calculations. The detection method is also more straightforward than the previously used impedance-based method as it measures the voltage response with a comparator to eliminate an ADC.

II. Architecture and Operation

A. Overview

Major functionalities of SHM include excitation signal generation, sensor actuation and sensing, and structural condition assessment. The excitation signal is transmitted to a self-sensing actuator, which is a piezoelectric material bonded to the target structure. The self-sensing actuator converts the received electric excitation signal into mechanical force to actuate the structure, and transforms the mechanical response of the structure back to an electric sensing signal. The sensing signal is measured and post processed for structural condition assessment. A digital signal processor (DSP) performs the excitation signal generation and structural condition assessment, and a PZT (Lead Zirconate Titanate) patch attached to the target structure operates as a self-sensing actuator.

Analog-based excitation techniques and impedance-based detection methods exploit a signal waveform represented in multiple voltage levels. Thus, DACs are normally located

1-4244-1053-3/07/$25.00 ©2007 IEEE.

between the DSP output and the self-sensing actuator input, and ADCs are required between the sensor output and the DSP input. However, as the proposed digital low-power approach employs a digital excitation technique and a sample-based detection method, both the DAC and ADC are eliminated. The absence of a DAC and ADC has noticeable advantage over the previous methods in physical size and power dissipation.

Figure 1 shows the overall architecture of the proposed digital low-power approach. The DPRT excitation signal produced by a pulse width modulation (PWM) signal generator of the DSP goes through two routes: a reference path and a measuring path. The reference path is a simple feedback path from the PWM output into a general purpose input/output (GPIO) port to provide the original excitation binary sequence. The measuring path includes the sensor actuation and sensing block utilizing an Opamp, as well as a comparator. The Opamp output, which is the structural response through the PZT, is quantized using a comparator to provide a binary sequence to the GPIO for DSP reception. Notice that we placed buffers between PWM output and GPIO input on the reference path and between PWM output and the PZT on the measuring path to avoid loading effects. Two binary input sequences, reference sequence and measuring sequence, are compared in the DSP for structural condition assessment.

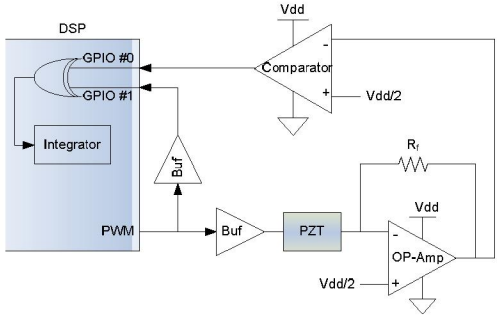

Figure 1 Overall architecture

B. *Digital Rectangular Pulse Train Generation*

An excitation signal is created to actuate the target structure within a certain frequency range for damage detection. The proposed digital low-power approach exploits a simple DRPT for excitation purposes. As shown in Figure 2, $|R(f)|$, the frequency response of a rectangular pulse $r(t)$, is similar to the sinc function shape. T_{full} and T_{duty} indicate the period and the duty cycle of a rectangular pulse $r(t)$, respectively. However, a repetition of rectangular pulses, DRPT $x_i(t)$, creates strong line spectrum at odd integer multiples of its repetition frequency, f_{full} (=1/ T_{full}), as illustrated in $|X_i(f)|$ of Figure 3. Therefore, by controlling the repetition frequency f_{full} of the rectangular pulse, we can create a signal with desired frequency components.

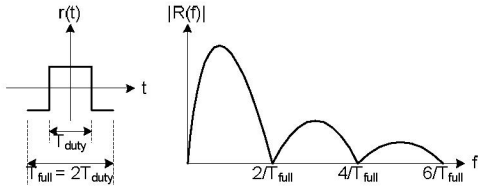

Figure 2 A rectangular pulse in the time and frequency domains

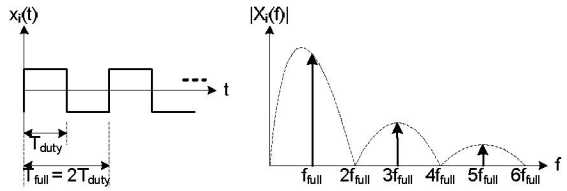

Figure 3 The DRPT in the time and frequency domains

For instance, assume the DSP operating clock frequency is 200 MHz, the detection frequency range is from 40 KHz to 50 KHz, and the excitation period for each frequency component is 2×10^5 DSP operating clock cycles, which is 1 msec. We can generate $x(t)$, consecutive DRPTs with frequency resolution of 1 KHz within the detection frequency range, as shown in Figure 4 (a). Then, $|X(f)|$, the frequency response of $x(t)$, has line spectrum in the 40 KHz to 50 KHz range with 1 KHz separation as shown in Figure 4 (b). As the signal level of the third harmonics appearing in the frequency range from 120 KHz to 150 KHz is 9.54 dB lower than the first harmonics, they will not significantly affect structural condition assessment performance in the detection frequency range. Moreover, we have observed that the mechanical structure usually does not respond to the excitation frequency over 100 KHz in our previous experiments [3]. Notice that the excitation time duration for each frequency component remains the same to excite the structure with the same amount of energy per frequency component.

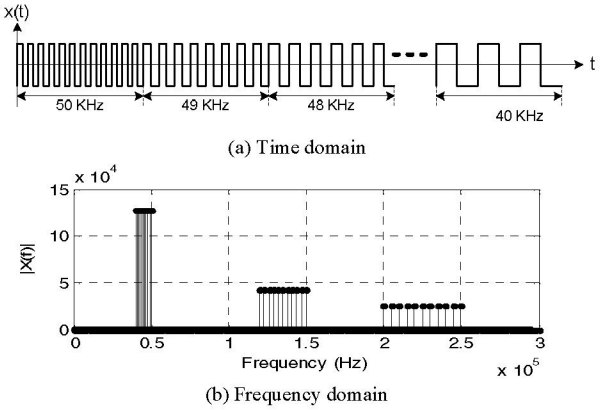

Figure 4 Example DRPT – Detection frequency range from 40 KHz to 50 KHz with 1 KHz frequency resolution

Keeping the duty cycle of the rectangular pulse as 50 % is important to effectively suppress the harmonics at DC and even integer multiples of its repetition frequency. Using an example duty cycle of 30 % as illustrated in Figure 5, the DRPT with anything other than a 50 % duty cycle spreads the energy on the odd harmonics over DC and even harmonics. The resulting excitation signal contains less energy than the DRPT with a 50 % duty cycle at the desired frequency and becomes vulnerable to background noise.

The generation of the DRPT excitation signal solely depends on the pulse width calculation for PWM output signal generation, which is a simple counting operation of DSP the operating clock cycles. Compared to the previous excitation techniques of [1] and [3], sinusoidal signal generation for sinc excitation waveform and random number generation for DW excitation signal are circumvented. Consequently, DSP performance requirements in terms of computational power

and operating clock frequency are relaxed in addition to the overall power and dimension gains from the elimination of the DAC.

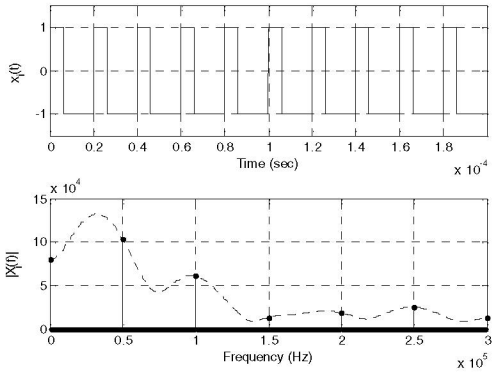

Figure 5 50 KHz DRPT with 30 % duty cycle

C. *Sensor Actuation and Sensing*

Once the DRPT excitation signal from the DSP reaches the self-sensing actuator, which is a PZT patch bonded to the structure, the structural response induces stress on the self-sensing actuator to produce an electrical sensing signal. The sensing signal is a representation of the structure's mechanical impedance, as it is altered from the original excitation signal according to the structure's mechanical impedance.

Previously, we proposed a linear excitation and sensing method that employs an Opamp with inverting gain and uses the PZT as a feedback resistance, as shown in Figure 6 [3]. In this configuration (Z-Configuration), the original excitation signal goes through an input resistor and the feedback signal from the Opamp excites the PZT bonded to the structure. Z-Configuration provides a linear response to the impedance of the PZT as expressed in equation (1).

$$v_{sense}(t) \approx -\frac{Z_{PZT}}{R_i} v_{excite}(t) \qquad (1)$$

Z_{PZT} indicates the impedance of the PZT, and R_i denotes the input resistor. v_{excite} and v_{sense} are the PWM output voltage from the DSP through a buffer and the input voltage to the comparator, respectively. Though the Z-Configuration generates a linear response to the impedance of the PZT, since the signal exciting the PZT is a feedback signal from the Opamp instead of the original PWM signal output generated by the DSP, the PZT excitation signal is unstable. The excitation signal has some unexpected frequency components in addition to the frequency components included in the digital rectangular pulse.

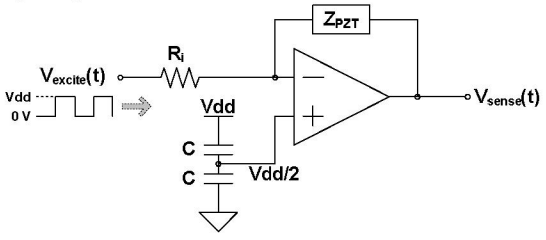

Figure 6 Excitation and Sensing: Z-Configuration

Therefore, an improved excitation and sensing configuration, Y-Configuration, is utilized as shown in Figure 7. In the Y-Configuration, the generated excitation signal by the DSP, instead of the feedback signal, is directed to the PZT. So that the PZT is excited with a rather clean and stable rectangular pulse with less unexpected frequency components. The Opamp's output signal, which is the structural response through the PZT, is linearly proportional to the admittance of the PZT as shown in equation (2).

$$v_{sense}(t) \approx -\frac{R_f}{Z_{PZT}} v_{excite}(t) \qquad (2)$$

Z_{PZT} indicates the impedance of PZT, and R_f denotes the feedback resistor. v_{excite} and v_{sense} are the PWM output voltage from the DSP through a buffer and the input voltage to the comparator, respectively.

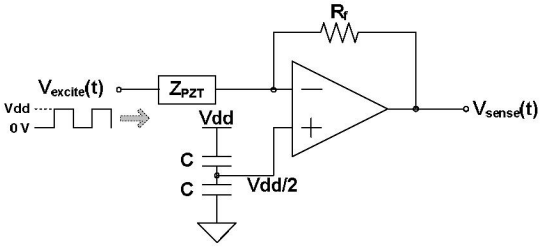

Figure 7 Excitation and Sensing: Y-Configuration

Since the generated DRPT v_{excite} swings between ground to supply voltage (Vdd), it contains a DC offset that is half of the supply voltage (Vdd/2). The DC offset cancellation is achieved by connecting the positive input end of the Opamp to Vdd/2, so that conversion from a uni-polar signal to a bipolar signal is eliminated. The positive input end of the comparator placed after the Opamp is also connected to Vdd/2 to provide a uni-polar signal to the GPIO of the DSP.

It is important to note that the proposed approach replaces a DAC and a power hungry ADC, which were necessary for the analog-based excitation of the impedance-based detection method, with a buffer and a comparator, respectively. These changes play a major role in hardware miniaturization and power reduction.

D. *Structural Condition Assessment*

The structural response sensed by the GPIO is post-processed to create a signature and calculate a damage metric for structural condition assessment. A signature is a frequency domain representation of the structural response that varies depending on the structure's mechanical impedance, and the first signature, called a baseline, is stored as a reference obtained from the healthy structure. As the DSP receives the reference signal and the measuring signal from two GPIOs, the variation on the DRPT excitation due to the structure's mechanical characteristics can be quantified by comparing those two binary sequences. Those two binary sequences, reference sequence and measuring sequence, are compared by exclusive-or (XOR) operation, and the XOR results are accumulated to obtain a variation count (VC). The VC at each frequency component within the detection frequency range constitutes a signature as expressed in equation (3).

$$\text{Signature: } VC(f) = \sum_{i=0}^{N_{sample}-1} XOR\left(S_{ref}(f,i), S_{msr}(f,i)\right) \qquad (3)$$

S_{ref} and S_{msr} indicate the reference sequence and measuring sequence, and N_{sample} is the number of received samples for

XOR and accumulation operation at each frequency component. Since the sensing voltage v_{sense} is proportional to the admittance of the structure as shown in equation (2) and quantized by a comparator, the deviation on the measuring sequence S_{msr} from the reference sequence S_{ref} mainly comes from the phase of the structure's admittance.

The damage metric is defined as an absolute sum of difference (ASD) between the baseline and the current VCs, as expressed in equation (4).

$$\text{Damage Metric: } ASD = \sum_{f=0}^{N_{freq}-1} \left| VC_B(f) - VC_C(f) \right| \quad (4)$$

VC_B is the baseline VC, and VC_C is the current VC. N_{freq} denotes the number of frequency components in the detection frequency range. When the structure stays in a healthy condition, the ASD value will remain under a certain threshold level. Upon occurrence of damage to the structure, the fresh VC diverges from the baseline due to the alteration on the mechanical impedance of the structure. When the increased ASD value becomes larger than a preset threshold value, the system indicates damage and warns the system operator.

As opposed to the previous impedance-based detection method of [1] and [3], the proposed method replaces memory-intensive ensemble average and computation-intensive FFT with a binary number accumulation on signature acquisition. Computational burden on damage metric calibration is also alleviated by adopting ASD instead of root mean squared deviation (RSMD). A simplified assessment procedure contributes to reducing the power dissipation at the DSP by adopting a low-performance DSP operating at a low clock frequency.

III. Performance Analisys

A. Test Structure and Preliminary Measurements

Figure 8 (a) shows a set of test structures, which are aluminum beams with a PZT bonded to one end. Three aluminum beams with the same dimensions but with different mechanical conditions are used. As a simulation of damage, two beams have different sized holes to alter the mechanical characteristics with varying amounts, while one beam is left without holes as a representation of a healthy condition. These three beams are connected to a rotary switch to easily connect to any of the beams. By using a switch with fixed damage, the simulated damage remains stable throughout the experiments. The detailed dimensions are provided in Figure 8 (b).

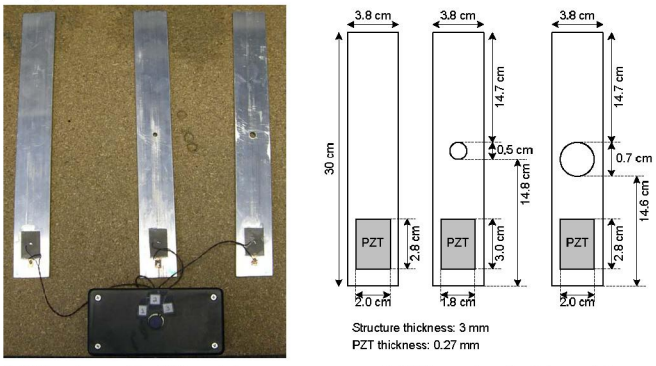

(a) Structure with different damage (b) Dimension (not in scale)

Figure 8 Test structure

Before the performance evaluation using the DSP prototype, we performed impedance measurements on the test structures using a HP 4194A impedance analyzer to determine the target frequency range and provide a performance reference. The impedance of each beam is measured from 100 Hz to 100 KHz with a frequency resolution of 10 Hz. To alleviate noise effects, 35 measurements were taken, and the maximally occurring value was selected at each frequency through a histogram analysis. Figure 9 (a) and (b) present the conductance and susceptance extracted from the measured impedance. Healthy, Damage 1, and Damage 2 indicate the three beams from left to right in Figure 8. It is noticeable that those three beams are sensitive to the excitation in the frequency ranges from 12 KHz to 25 KHz and from 68 KHz to 76 KHz. The higher detection frequency requires a faster operating clock on generating the excitation signal, which in turn increases the power dissipation. Hence, the frequency range from 12 KHz to 25 KHz is chosen as a target detection frequency range.

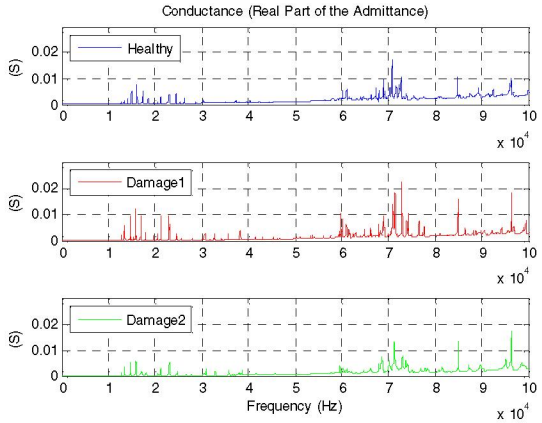

(a) Conductance

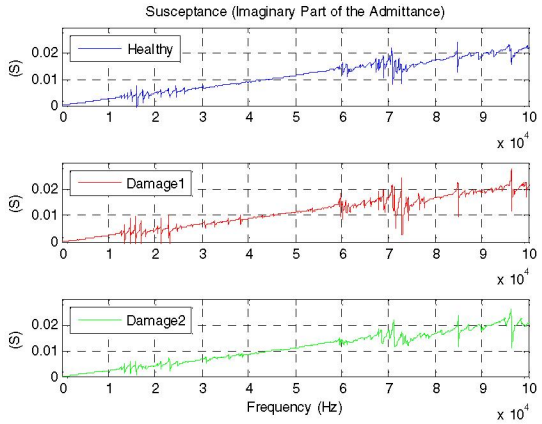

(b) Susceptance

Figure 9 Admittance from the impedance analyzer measurement data

RMSD values, the damage metric generally used in impedance-based SHM, of Damage 1 and Damage 2 are also calculated based on the admittance from the measured impedance as a reference performance for the verification purposes. The real part of the admittance is used as it reflects the structural damage more clearly than the imaginary part of the admittance [4]. The calculated RMSD value for Damage 1

is 14.214×10^{-4} and that for Damage 2 is 9.710×10^{-4}. Therefore, the DSP prototype is expected to provide larger damage metric for Damage 1 than Damage 2, as well as a larger damage metric for damaged structures than the healthy structure.

The feedback resistor R_f for excitation and sensing configuration shown in Figure 7 is selected as 100 Ω, based on the magnitude of the measured impedance within the selected detection frequency range. The magnitude of the impedance for the Healthy beam in the detection frequency range varies from 70 Ω to 1137 Ω, and a 95 % confidence interval is from 103 Ω to 399 Ω. As expressed in equation (2), the gain of the Opamp is R_f / Z_{PZT}, and the Opamp negative input voltage v_{excite} swings between 0 V and Vdd. Thus, to keep the excitation and sensing configuration operating as a rational amplifier, R_f is selected as 100 Ω, which is the lower boundary of the 95 % confidence interval maintaining the amplifier gain of less than unity.

B. DSP Prototype Measurements and Validation

As shown in Figure 10, the prototype is developed from a TI DSP EVM with the TMS320F2812 [5], which is a 32-bit fixed point DSP, and a couple of TI Opamps, which are OPA4342 [6] and TLV2770 [7]. Three channels of the OPA4342 are used for implementing two buffers and a comparator, and the TLV2770 is employed for PZT excitation and sensing configuration. Miscellaneous components such as resistors and an LED are also included.

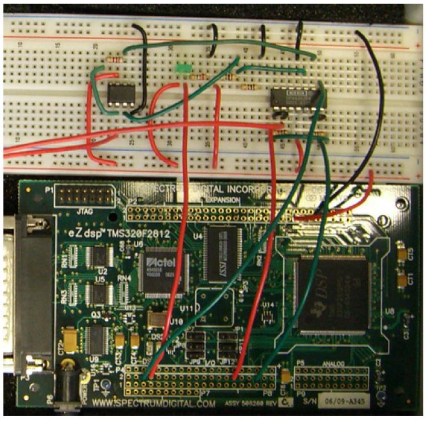

Figure 10 Prototype using TMS320F2812 EVM

In order to verify the operation and estimate the performance of the proposed digital low-power approach, a set of measurements has been taken. The test structure shown in Figure 8 is employed, and the detection frequency range and feedback resistor size found from the preliminary impedance measurements are used. For the experiment, the operating clock frequency of the DSP and the average frequency resolution are set as 150 MHz and 20 Hz, respectively.

The measured VC at each frequency component is shown in Figure 11. By comparing the waveform of the VC from the proposed digital low-power approach with the admittance phase from the impedance measurement data shown in Figure 12, we can observe that the VC waveform follows the trajectory of the admittance phase. The correlation coefficients between VC and admittance phase and between VC and admittance magnitude summarized in TABLE I also confirm that the VC has higher correlation with the admittance phase than with the admittance magnitude.

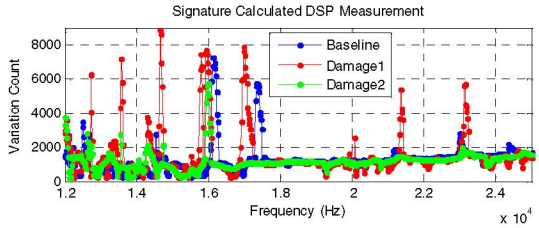

Figure 11 DSP measurement data – signature using the test structure

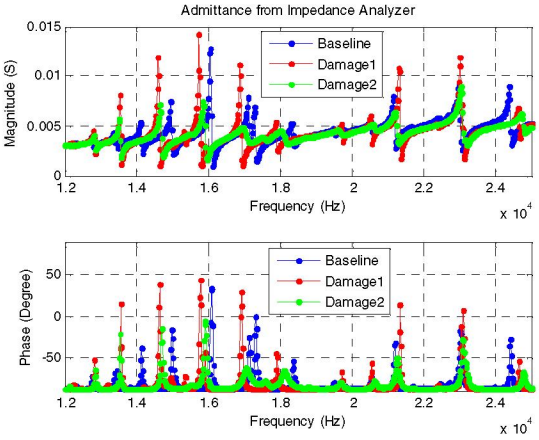

Figure 12 Admittance calculated from the measured impedance – magnitude and phase

TABLE I CORRELATION COEFFICIENT – VC VS. ADMITTANCE

	VC vs. Phase	VC vs. Magnitude
Baseline	0.3549	-0.1572
Damage1	0.4730	-0.2882
Damage2	0.1886	-0.0622

Since the proposed digital low-power approach utilizes admittance phase in damage detection as opposed to the traditional impedance-based detection method that uses the real part of the admittance, the correlation between the phase / magnitude of the admittance and real / imaginary parts of the admittance are examined for the sake of validation. As shown in Figure 12 and Figure 13, just by observing the waveforms, we can notice that admittance phase follows admittance real part, and admittance magnitude follows admittance imaginary part. Correlation coefficients of real and phase (CCRP) and correlation coefficients of imaginary and magnitude (CCIM) of the admittance are summarized in TABLE II with three structural conditions. The absolute values of CCRP and CCIM are larger than 0.7 for all three structural conditions. Therefore, we can confirm that exploiting the admittance phase instead of real part of the admittance is a valid damage detection method.

TABLE II CORRELATION COEFFICIENT OF ADMITTANCE

	Real vs. Phase	Imaginary vs. Magnitude
Baseline	0.7895	-0.8156
Damage1	0.7161	-0.7077
Damage2	0.8810	-0.9186

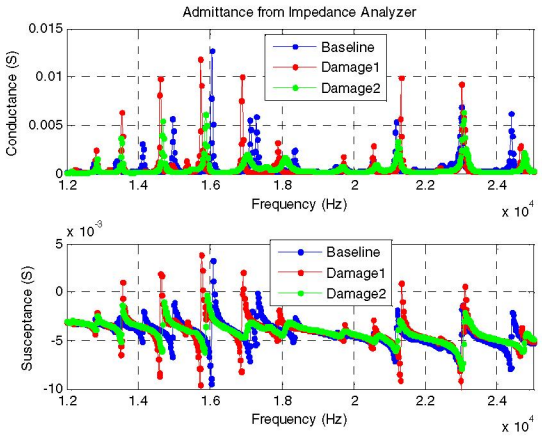

Figure 13 Admittance calculated from the measured impedance – real and imaginary

C. *Performance*

The ASD damage metric obtained from the DSP prototype implementing the proposed digital low-power approach is compared with RMSD calculated from the impedance analyzer measurement data as summarized in TABLE III. The same test setup covered in Sections III.A and III.B is used. Clearly, the proposed digital low-power approach can detect the damage on the structure as the ASD value is six to ten times larger for damaged structures than for the healthy structure. Also, it is noticeable that the proposed approach can distinguish different damages, because the ASD value is larger for Damage 1 than Damage 2 as predicted by the RMSD values calculated from the impedance analyzer measurement data.

TABLE III DAMAGE DETECTION PERFORMANCE COMPARISON

Damage	**Damage Metric**	
	Measured Impedance (RMSD)	***Proposed Approach (ASD)***
None (Healthy)	N/A	52760
Damage 1	14.214×10^{-4}	544613
Damge 2	9.710×10^{-4}	309816

Power dissipation measured with two operating clock frequencies is presented in TABLE IV. Assuming that the structure remains without damage most of the time, the damage indication LED will stay off. Therefore, the typical power dissipation is 1.7 W with the default 150 MHz operating clock frequency, and 790 mW with the minimum 15 MHz operating clock frequency.

TABLE IV OPERATING CLOCK FREQUENCY AND POWER DISSIPATION

Operating Clock Frequency (MHz)	**Power Consumption (mW)**	
	LED Off	***LED On***
150	1715	1820
15	790	900

As summarized in TABLE V, the proposed digital low-power approach consumes only 20 % and 24 % of the total power dissipation of the previous sinc excitation and WD excitation with impedance-based detection method. The major power reduction comes from the elimination of the DAC and ADC by employing digital signals on both structural excitation and sensing. The simplified structural condition assessment procedure also reduces the power consumed by the DSP itself in half.

TABLE V POWER DISSIPATION COMPARISON

Component	**Power Dissipation (W)**		
	Sinc Approach	***DW Approach***	***Proposed Digital Low-Power Approach***
DSP	1.58	1.58	0.79
DAC	0.75	N/A	N/A
ADC	1.68	1.68	N/A
Total	4.01	3.26	0.79

IV. SUMMARY AND CONCLUSION

We have proposed a digital low-power SHM approach utilizing a DRPT excitation signal and a sample-based detection method to reduce power dissipation and miniaturize the hardware by eliminating the usage of a DAC and an ADC. These improvements can be achieved by simplifying the excitation and damage detection algorithm. Compared to the impulse-like sinc wave excitation employed in our first prototype, the proposed digital low-power approach reduces the power dissipation by 80 %. The measurement results obtained from the prototype are compared with results collected from a traditional impedance analyzer. Results of this comparison showed the proposed digital low-power approach provides a reliable means of detecting damage as compared with impedance analyzer measurement data.

ACKNOWLEDGMENT

This material is based upon work supported by the National Science Foundation under Grant No. 0426777. Any opinions, findings, and conclusions or recommendations expressed in this material are those of the authors and do not necessarily reflect the views of the National Science Foundation.

REFERENCES

[1] B.L. Grisso and D.J. Inman, "Developing an Autonomous On-Orbit Impedance-Based SHM for Thermal Protection Systems," *International Workshop on Structural Health Monitoring*, pp. 435-442, September 2005.

[2] D.J. Inman and B.L. Grisso, "Towards Autonomous Sensing," *SPIE International Symposium on Smart Structures and Materials*, vol. 6174, pp. 248-254, February 2006.

[3] J. Kim, B.L. Grisso, D.S. Ha, and D.J. Inman, "Digital Wideband Excitation Technique for Impedance-Based Structurla Health Monitoring Systems," *IEEE Internatinal Symposium on Circuits and Systems*, May 2007.

[4] G. Park, H. Sohn, C.R. Farrar, and D.J. Inman, "Overview of Piezoelectric Impedance-Based Health Monitoring and Path Forward," *The Shock and Vibration Digest*, vol. 35, no. 6, pp. 451-463, November 2003.

[5] TMS320F2812 Digital Signal Processor Data Manual, Texas Instruments Inc., May 2006.

[6] OPA4342 Low-Cost, Low-Power, Rail-to-Rail Operational Amplifiers, Texas Instruments Inc., August 2000.

[7] TLV277x Family of 2.7-V High-Slew-Rate Rail-to-Rail Output Operational Amplifiers with Shutdown, Texas Instruments Inc., February 2004.